

Strong coupling analysis of the large- N 2-d lattice chiral models.

Massimo Campostrini, Paolo Rossi, and Ettore Vicari

Dipartimento di Fisica dell'Università and I.N.F.N., I-56126 Pisa, Italy

Two dimensional $N = \infty$ chiral models on the square and honeycomb lattices are investigated by a strong coupling analysis. Strong coupling expansion turns out to be predictive for the evaluation of continuum physical quantities, to the point of showing asymptotic scaling. Indeed in the strong coupling region a quite large range of β values exists where the fundamental mass agrees, within about 5% on the square lattice and about 10% on the honeycomb lattice, with the continuum predictions in the energy scheme.

PACS numbers: 11.15 Ha, 11.15 Pg, 75.10 Hk

arXiv:hep-lat/9412101v1 24 Dec 1994

I. INTRODUCTION

Recent numerical studies of lattice two-dimensional $SU(N) \times SU(N)$ principal chiral models, with the standard nearest-neighbour interaction

$$S_L = -2N\beta \sum_{x,\mu} \text{Re Tr} [U(x) U^\dagger(x+\mu)] , \quad \beta = \frac{1}{NT} , \quad (1)$$

have shown the existence of a scaling region, where continuum predictions for dimensionless ratios of physical quantities are substantially verified [1,2]. The scaling region begins at relatively small values of the correlation length well within the expected region of convergence of strong-coupling expansion. Moreover by performing a variable change [7] from the temperature T to

$$T_E = \frac{8N}{N^2 - 1} E , \quad \beta_E = \frac{1}{NT_E} , \quad (2)$$

where E is the internal energy, one can find agreement in the whole scaling region between the measured mass scale and the asymptotic scaling prediction, within few per cent [2].

As a matter of fact, this may be considered as an evidence for asymptotic scaling within the strong-coupling regime, motivating a test of scaling and asymptotic scaling by strong coupling computations. As a byproduct, strong-coupling series can be analyzed to investigate the critical behavior of the $N = \infty$ theory, where Monte Carlo data seem to indicate the existence of a phase transition at finite β .

Ref. [4] was devoted to a complete presentation of our strong coupling calculations performed by means of the character expansion. We calculated strong coupling series for several quantities on the square and honeycomb lattices. On the ordinary square lattice, we calculated the free energy up to $O(\beta^{18})$, and the fundamental Green's function

$$G(x) = \langle \frac{1}{N} \text{Re Tr} [U(x)U(0)^\dagger] \rangle \quad (3)$$

up to $O(\beta^{15})$. For chiral models on the honeycomb lattice, defined by the nearest-neighbour action, longer series were obtained: the free energy up to $O(\beta^{26})$ and $G(x)$ up to $O(\beta^{20})$. Lattice chiral models on square and honeycomb lattices are expected to belong to the same class of universality with respect to the continuum limit. As we will see from the strong coupling analysis, even at finite β large- N chiral models on the honeycomb lattices show a pattern very similar to that observed on the square lattice.

In this paper, which represents the logical continuation of Ref. [4], we analyze the $N = \infty$ strong coupling series presented there and the results are compared with the continuum limit predictions and Monte Carlo simulations. The main result of our strong coupling analysis of 2-d $N = \infty$ chiral models on the square and honeycomb lattices is the identification of a scaling region where known continuum results are reproduced with good accuracy, and asymptotic predictions are substantially fulfilled in the energy scheme.

II. STRONG COUPLING EVIDENCE OF A LARGE- N PHASE TRANSITION.

Numerical simulations at large N of $SU(N)$ and $U(N)$ lattice chiral models show evidence of a phase transition at $N = \infty$. Indeed sharper and sharper peaks in the specific heat

$$C = \frac{1}{N} \frac{dE}{dT} \quad (4)$$

are observed with increasing N , suggesting a divergent large- N limit at a finite β [2]. By extrapolating to $N = \infty$ the positions of the specific heat peaks, we obtained a rather precise estimate of the critical coupling: $\beta_c = 0.3057(3)$. Details on our Monte Carlo simulations and their analysis can be found in Ref. [5].

In order to investigate the above issue, we analyze the $N = \infty$ strong coupling series by employing the integral approximant technique [9,10], which is especially recommended in the case of small critical exponent [11]. The method of integral approximants consists of representing the power series under study by the integral of a linear differential equation. In our analysis we considered the integral approximants obtained from a first order linear differential equation

$$Q_L(x)f'(x) + P_K(x)f(x) + R_J(x) = O(x^{L+K+J+2}), \quad (5)$$

where Q_L, P_K and R_J are respectively L, K , and J order polynomials (we fix $Q_{L,0} = 1$). These approximants are singular at the zeroes x_0 of $Q_L(x)$, and behave as

$$A(x)|x - x_0|^{-\gamma} + B(x), \quad (6)$$

where $A(x)$ and $B(x)$ are regular in the neighbourhood of x_0 , and

$$\gamma = -\frac{P_K(x_0)}{Q'_L(x_0)}. \quad (7)$$

Given a M order series, L, K and J must satisfy the condition $L + K + J + 2 \leq M$.

Let us analyze the $N = \infty$ strong coupling series of the specific heat, which is even in β :

$$\begin{aligned} \beta^{-2}C &= 1 + 6x + 30x^2 + 266x^3 + 2160x^4 + 19932x^5 \\ &+ 183638x^6 + 1754130x^7 + 16911192x^8 + O(x^9), \end{aligned} \quad (8)$$

where $x = \beta^2$. In Table I we report the first singularity in the real axis and the corresponding exponent for different values of L, K , and J . The results are quite stable, leading to a critical behavior of the specific heat typical of a second order phase transition:

$$C \sim |\beta - \beta_c|^{-\alpha}. \quad (9)$$

From Table I we estimate

$$\begin{aligned} \beta_c &= 0.3058(3), \\ \alpha &= 0.23(3). \end{aligned} \quad (10)$$

The errors are just indicative. They are the variance of the results in Table I after discarding the two furthest values from the corresponding average; they should give an idea of the spread of the results coming from different approximants. Notice that the strong coupling determination of β_c is in agreement with its estimate from numerical simulations at large N .

As further check of the above resummation procedure, Fig. 1 compares, in the region $\beta < \beta_c$, $SU(N)$ and $U(N)$ Monte Carlo data of the specific heat at large N ($N = 21, 30$ for $SU(N)$, and $N = 15, 21$ for $U(N)$) with the determinations coming from the resummed and the plain strong coupling series (8). We recall that $SU(N)$ and $U(N)$ models should have the same large- N limit. Monte Carlo data of C appear to approach, for growing N , the determination from the resummed strong coupling series. As expected from simple considerations on the finite N corrections to the $N = \infty$ strong coupling series, $U(N)$ models converge faster than $SU(N)$ models to the $N = \infty$ limit in the strong coupling region.

Monte Carlo data at large N seem to indicate that all physical quantities, such as the magnetic susceptibility $\chi \equiv \sum_x G(x)$ and the second moment mass M_G^2 ($M_G \equiv 1/\xi_G$ and $\chi\xi_G^2 \equiv \frac{1}{4}\sum_x x^2 G(x)$), are well behaved functions of the internal energy even at $N = \infty$ [2]. Therefore, as a consequence of the specific heat divergence, χ and M_G^2 should have a singular behavior with respect to β . We indeed expect

$$\frac{d \ln \chi}{d\beta} \sim \frac{d \ln M_G^2}{d\beta} \sim |\beta - \beta_c|^{-\alpha}. \quad (11)$$

in the neighbourhood of β_c . Notice that a behavior like Eq. (11) leads to a non-analytical zero of the β -function $\beta_L(T)$ at β_c :

$$\beta_L(T) \sim |\beta - \beta_c|^\alpha \quad (12)$$

around β_c , explaining the observed behavior with respect to β of the large- N Monte Carlo data for the fundamental mass [2].

In order to check the behavior (11), we analyzed the corresponding strong coupling series by a modified integral approximant scheme forcing the approximant to have a singularity at $\beta \simeq 0.3058$, obtaining biased estimates of the exponent in Eq. (11). In this modified scheme the values of L, K , and J in Eq. (5) must be chosen according to the condition $L + K + J + 1 \leq M$. We analyze the series

$$\begin{aligned} \frac{d \ln \chi}{d\beta} = & 4 + 8\beta + 28\beta^2 + 48\beta^3 + 204\beta^4 + 440\beta^5 + 1740\beta^6 + 3744\beta^7 + 15148\beta^8 + 35048\beta^9 \\ & + 140980\beta^{10} + 327600\beta^{11} + 1323612\beta^{12} + 3149112\beta^{13} + 12727908\beta^{14} + O(\beta^{15}), \end{aligned} \quad (13)$$

and

$$\begin{aligned} \frac{d \ln \beta M_G^2}{d\beta} = & -4 - 10\beta - 28\beta^2 - 74\beta^3 - 224\beta^4 - 598\beta^5 - 1936\beta^6 - 5282\beta^7 - 17560\beta^8 \\ & - 49170\beta^9 - 162144\beta^{10} - 464426\beta^{11} - 1549656\beta^{12} - 4459234\beta^{13} + O(\beta^{14}). \end{aligned} \quad (14)$$

In Table II we report the range of the exponent variations when varying the zero in the interval $0.3055 - 0.3061$. These results are quite consistent with the exponent α obtained

in the analysis of the specific heat strong coupling series, supporting the relations (11) and therefore (12). When performing an unbiased analysis of the series (13) and (14), that is without forcing the approximants to have a zero at a fixed β , the singularity and the corresponding exponent turn out to be less stable; more terms in the series would be necessary to have a satisfactory analysis independent of that of the specific heat.

In Fig. 2 we compare our strong coupling calculations of χ with the Monte Carlo data of $SU(N)$ and $U(N)$ models at large N . An improved strong coupling estimate of χ , represented by the full line in Fig. 2, was obtained by integrating the resummed series of $d \ln \chi / d\beta$ (using $L = 5$, $K = 4$ and $J = 4$, see Table II). Growing N , the $SU(N)$ and $U(N)$ data of χ and ξ_G approach the same $N = \infty$ limit, which is well reproduced by the resummation of the series (13) and (14) in the strong coupling region.

We should mention an apparent discrepancy between the $SU(N)$ Monte Carlo results at large N and the resummation of the $N = \infty$ series. In the $SU(N)$ numerical simulations, when varying N (for sufficiently large N) the position of the peak of the specific heat turns out to be quite stable with respect to the correlation length, $\xi_G^{peak} \simeq 2.8$, leading to the expectation that at the large- N critical point $\xi_G^{(c)} \simeq 2.8$ [2]. On the other hand the estimate of ξ_G from the resummation of the strong coupling series is slightly smaller: $\simeq 2.5$.

III. SCALING AND ASYMPTOTIC SCALING.

In spite of the existence of a phase transition at $N = \infty$, Monte Carlo data at large N showed scaling and approximate asymptotic scaling (in the energy scheme) even for β smaller than the peak of the specific heat [2]. The stability of this pattern suggests an effective decoupling of the modes responsible for the phase transition from those determining the physical continuum limit, and therefore that evidences of scaling and asymptotic scaling could be provided by the large- N strong coupling expansion.

The on-shell fundamental mass M can be extracted from the long distance behavior of the correlation function in the fundamental channel $G(x)$, or from the imaginary pole of its Fourier transform. We considered two estimators of M , μ_s and μ_d , defined from the long distance behavior of wall-wall correlation functions constructed with $G(x)$ respectively along the sides and the diagonals of the lattice. An alternative mass M_G is defined from the inverse second moment of $G(x)$. Unlike the on-shell mass M , M_G is an off-shell quantity, it is related to the zero momentum of the Fourier transform of $G(x)$, indeed $\tilde{G}(p)^{-1} \sim M_G^2 + p^2$ at small momentum.

The quantities μ_s , μ_d and M_G^2 enable us to perform tests of scaling based on rotational invariance at distances $d \gtrsim \xi \equiv 1/\mu_s$, checking $\mu_s/\mu_d \simeq 1$, and on the stability of dimensionless physical quantities, looking at the ratio μ_s/M_G . We should say that these tests concern the long distance physics of chiral models.

Monte Carlo data at relatively large N showed that, within statistical errors of few per mille, the above scaling requirements are verified already at $\xi \simeq \xi_G \simeq 2$, well within the strong coupling region. Numerical simulations provided an estimate of the large- N limit of the ratio M/M_G in the continuum limit: $M/M_G = 0.991(1)$ [2].

In Ref. [4] the strong coupling series corresponding to the above mentioned quantities have been calculated, in particular M_G^2 up to $O(\beta^{13})$, $M_s^2 \equiv 2(\cosh \mu_s - 1)$ up to $O(\beta^{11})$,

and $M_d^2 \equiv 4(\cosh \mu_d/\sqrt{2} - 1)$ up to $O(\beta^{10})$.

In Fig. 3 we plot the ratio μ_s/μ_d vs. the correlation length $\xi_G \equiv 1/M_G$ as obtained from our strong coupling series. The $N = \infty$ strong coupling curve confirms the large- N Monte Carlo result: $\mu_s/\mu_d \simeq 1$ within few per mille at $\xi \simeq 2$.

Fig. 4 shows the ratio μ_s/M_G vs. ξ_G . Notice the stability of the curve for a large region of values of ξ_G and the good agreement (well within 1%) with the continuum large- N value extrapolated by Monte Carlo data.

In order to test asymptotic scaling we perform the variable change indicated in Eq.(2), evaluating the energy from its strong-coupling series. The two loop renormalization group and a Bethe Ansatz evaluation of the mass Λ -parameter ratio [8] lead to the following large- N asymptotic scaling prediction for the on-shell fundamental mass in the β_E scheme:

$$\begin{aligned} M &\cong R_E \Lambda_{E,2l}(\beta_E) , \\ R_E &= 16\sqrt{\frac{\pi}{e}} \exp\left(\frac{\pi}{4}\right) , \\ \Lambda_{E,2l}(\beta_E) &= \sqrt{8\pi\beta_E} \exp(-8\pi\beta_E) , \\ \beta_E &= \frac{1}{8E} . \end{aligned} \tag{15}$$

In Fig. 5 the strong-coupling estimates of $\mu_s/\Lambda_{E,2l}$ and $M_G/\Lambda_{E,2l}$ are plotted vs. β_E , for a region of coupling corresponding to correlation lengths $1.5 \lesssim \xi_G \lesssim 3$. (We recall that M_G differs from M by about 1% in the continuum limit.) The agreement with the exact continuum prediction is within about 5% in the whole region. Notice also that both curves go smoothly through the value of β_E corresponding to the specific heat singularity β_c , which is $\beta_E^{(c)} \simeq 0.220$.

The strong coupling curves in Fig. 5 were obtained from the plain series of the energy and respectively of M_s^2 and M_G^2 . In the case of M_G , we also determined $M_G/\Lambda_{E,2l}$ evaluating the energy and M_G^2 by integrating the resummed series respectively of the specific heat and of $d \ln \beta M_G^2/d\beta$. The resulting curve changes very little from that derived from the plain series, the difference between the two curves would not be visible in Fig. 5. This indicates once more that the change of variable $\beta \rightarrow \beta_E$ washes out the singularity in β when considering physical quantities.

IV. CHIRAL MODELS ON THE HONEYCOMB LATTICE.

On the honeycomb lattice we consider the action with nearest-neighbour interaction. It can be written as a sum over all links of the honeycomb lattice:

$$S_h = -2N\beta \sum_{\text{links}} \text{Re Tr} [U_l U_r^\dagger] , \quad U \in SU(N) , \tag{16}$$

where l, r indicate the sites at the ends of each link. As on the square lattice, a lattice space a , which represents the lattice length unit, is defined to be the length of a link. The volume of an hexagon is $v_h = 3\sqrt{3}/2$. Straightforward calculations show that the correct continuum limit is obtained identifying

$$T = \frac{\sqrt{3}}{N\beta}. \quad (17)$$

A. The large- N phase transition.

On the honeycomb lattice we have calculated the $N = \infty$ strong coupling series of the specific heat, which is even in β , up to 26th order in β :

$$\begin{aligned} \beta^{-2}C = & 1 + 10x^2 + 90x^4 + 396x^5 + 728x^6 + 9120x^7 + 28186x^8 + 136800x^9 \\ & + 886116x^{10} + 3129380x^{11} + 18935800x^{12} + O(x^{13}), \end{aligned} \quad (18)$$

where $x = \beta^2$. The integral approximant analysis of the above series, whose results are reported in Table III, leads again to a second order type critical behavior with the following estimates of the critical β and α exponent:

$$\begin{aligned} \beta_c &= 0.4339(1), \\ \alpha &= 0.17(1). \end{aligned} \quad (19)$$

Notice that this estimate of the exponent α is very close to that of the square lattice. The uncertainty on both estimates cannot really exclude that they are equal, which would be an indication of universality.

Also in this context we analyzed the strong coupling series of the logarithmic derivative of the magnetic susceptibility χ and βM_G^2 by the modified integral approximant method which forces the existence of a zero at β_c . In Table II we report the range of the exponent variations when varying the zero in the interval 0.4338 – 0.4340. As for the square lattice, the results in Table II are consistent with a divergence characterized by the specific heat exponent (cfr. Eq. (11), supporting the existence of a non-analytical zero of the β -function at β_c .

B. Scaling.

On the hexagonal lattice the maximal violation of the full rotational symmetry occurs for directions differing by a $\pi/6$ angle, and therefore, taking into account its discrete rotational symmetry, also by a $\pi/2$ angle. So a good test of rotation invariance is provided by the ratio between masses extracted from the long distance behaviors of a couple of orthogonal wall-wall correlation functions constructed with $G(x)$.

In Ref. [4] we defined two orthogonal wall-wall correlation functions $G_1^{(w)}(x)$ and $G_2^{(w)}(x)$, with the corresponding masses μ_1 and μ_2 , which should both reproduce the on-shell fundamental mass M in the continuum limit. In order to extract μ_1 and μ_2 we evaluated the $O(\beta^{18})$ series of $\exp(-3\mu_1/2)$ and the $O(\beta^{17})$ series of $\exp(-\sqrt{3}\mu_2/2)$.

Fig. 6 shows the ratio μ_1/μ_2 vs. $\xi_G \equiv 1/M_G$. As expected from the better rotational symmetry of the honeycomb lattice, rotation invariance is set earlier than for the square lattice: already at a correlation length $\xi_G \simeq 0.5$ $\mu_1/\mu_2 \simeq 1$ within 1%.

In Fig. 7 we plot the ratio μ_1/M_G vs. ξ_G . The approach to the continuum limit value seems to be substantially equivalent to that observed on the square lattice, but then for $\xi_G \gtrsim 1.5$ the curve becomes unstable. Such an instability should be cured by an extension of the series.

C. Asymptotic scaling.

The asymptotic scaling test is again best performed in the energy scheme. This requires some weak coupling calculations, which present some subtleties on the honeycomb lattice. This is essentially due to the fact that, unlike square and triangular lattices, lattice sites are not characterized by a group of translations. Details on our weak coupling calculations are given in the Appendix.

We calculated the internal energy (per link) up to two loops, finding

$$E = \frac{N^2 - 1}{N} \frac{T}{6\sqrt{3}} \left[1 + \frac{N^2 - 2}{N} \frac{T}{24\sqrt{3}} + O(T^2) \right]. \quad (20)$$

The energy scheme consists in defining a new temperature T_E proportional to the energy

$$T_E = \frac{6\sqrt{3}N}{N^2 - 1} E, \quad \beta_E = \frac{1}{NT_E}. \quad (21)$$

The other important ingredient in this game is the mass Λ -parameter ratio in the honeycomb lattice regularization, which requires the calculation of the ratio between the Λ -parameter of the \overline{MS} renormalization scheme $\Lambda_{\overline{MS}}$ and that of the honeycomb lattice regularization Λ_h , given that the (on-shell) mass Λ -parameter ratio in the \overline{MS} scheme is known [8].

From a one loop calculation we obtained

$$\frac{\Lambda_{\overline{MS}}}{\Lambda_h} = 4 \exp\left(\frac{N^2 - 2}{N^2} \frac{2\pi}{3\sqrt{3}}\right). \quad (22)$$

The ratio between $\Lambda_{h,E}$, the Λ parameter of the energy scheme, and Λ_h is easily obtained from the two loop term of the internal energy:

$$\frac{\Lambda_h}{\Lambda_{h,E}} = \exp\left(-\frac{N^2 - 2}{N^2} \frac{\pi}{3\sqrt{3}}\right). \quad (23)$$

Then the $N = \infty$ asymptotic scaling prediction in the energy scheme is

$$\begin{aligned} M &\cong R_{h,E} \Lambda_{E,2l}(\beta_E), \\ R_{h,E} &= 8\sqrt{\frac{2\pi}{e}} \exp\left(\frac{\pi}{3\sqrt{3}}\right), \\ \Lambda_{E,2l}(\beta_E) &= \sqrt{8\pi\beta_E} \exp(-8\pi\beta_E), \\ \beta_E &= \frac{1}{6\sqrt{3}E}. \end{aligned} \quad (24)$$

Fig. 8 shows the ratios $\mu_1/\Lambda_{E,2l}$ and $M_G/\Lambda_{E,2l}$ vs. β_E (corresponding to correlation lengths $1 \lesssim \xi_G \lesssim 2.5$), as obtained from the corresponding strong coupling series. Again there is good agreement with the continuum prediction, especially in the region corresponding to correlation length $\xi_G \gtrsim 2$, where the agreement is within 10%. The curve corresponding to M_G is more stable, and it changes little when calculated resumming the involved series.

APPENDIX A: WEAK COUPLING EXPANSION ON THE HONEYCOMB LATTICE.

On the honeycomb lattice the sites cannot be associated to a group of translation. This causes a few subtleties in the analysis of models on such a lattice.

The sites \vec{x} of a finite periodic hexagonal lattice can be represented in cartesian coordinates by

$$\begin{aligned} \vec{x}(l_1, l_2, l_3) &= l_1 \vec{\eta}_1 + l_2 \vec{\eta}_2 + l_3 \left(\frac{1}{2}, 0 \right), \\ l_1 &= 1, \dots, L_1, \quad l_2 = 1, \dots, L_2, \quad l_3 = -1, 1, \\ \vec{\eta}_1 &= \left(\frac{3}{2}, \frac{\sqrt{3}}{2} \right), \quad \vec{\eta}_2 = (0, \sqrt{3}). \end{aligned} \tag{A1}$$

We set $a = 1$, where the lattice space a is the length of a link. The total number of exagons on the lattice is $L_1 L_2$, while the sites are $2L_1 L_2$. The coordinate l_3 can be interpreted as the parity of the corresponding lattice site: sites with the same parity are connected by an even number of links.

Notice that each of the two sublattices identified by $\vec{x}_-(l_1, l_2) \equiv \vec{x}(l_1, l_2, -1)$ and $\vec{x}_+(l_1, l_2) \equiv \vec{x}(l_1, l_2, 1)$ forms a triangular lattice. Each link of the honeycomb lattice connects sites belonging to different sublattices. Triangular lattices have a more symmetric structure, in that their sites are characterized by a group of translations. It is then convenient to rewrite a field $\phi(\vec{x}) \equiv \phi(l_1, l_2, l_3)$ in terms of two new fields $\phi_-(\vec{x}_-) \equiv \phi(\vec{x}_-)$ and $\phi_+(\vec{x}_+) \equiv \phi(\vec{x}_+)$ defined respectively on the sublattices \vec{x}_- and \vec{x}_+ . A finite lattice Fourier transform can be consistently defined

$$\begin{aligned} \phi_{\pm}(\vec{p}) &= v_h \sum_{\vec{x}_{\pm}} e^{i\vec{p} \cdot \vec{x}_{\pm}} \phi_{\pm}(\vec{x}_{\pm}), \\ \phi_{\pm}(\vec{x}_{\pm}) &= \frac{1}{v_h L_1 L_2} \sum_{\vec{p}} e^{-i\vec{p} \cdot \vec{x}_{\pm}} \phi_{\pm}(\vec{p}), \end{aligned} \tag{A2}$$

where $v_h = 3\sqrt{3}/2$ is the volume of an hexagon, and the set of momenta is

$$\begin{aligned} \vec{p} &= \frac{2\pi}{L_1} m_1 \vec{\rho}_1 + \frac{2\pi}{L_2} m_2 \vec{\rho}_2 \\ m_1 &= 1, \dots, L_1, \quad m_2 = 1, \dots, L_2, \\ \vec{\rho}_1 &= \left(\frac{2}{3}, 0 \right), \quad \vec{\rho}_2 = \left(-\frac{1}{3}, \frac{1}{\sqrt{3}} \right). \end{aligned} \tag{A3}$$

Notice that

$$\vec{p} \cdot \vec{x} = \frac{2\pi}{L_1} l_1 m_1 + \frac{2\pi}{L_2} l_2 m_2 + l_3 \frac{p_1}{2}. \quad (\text{A4})$$

To begin with, let us discuss the simple Gaussian models, whose action can be written as

$$S_G = \frac{\kappa}{2} \sum_{\text{links}} (\phi(x_l) - \phi(x_r))^2 \quad (\text{A5})$$

where x_l, x_r indicate the sites at the ends of each link. Rewriting the field $\phi(x)$ in terms of two fields $\phi_-(x_-)$ and $\phi_+(x_+)$ as described above, and performing the Fourier transform (A2) we obtain

$$S_G = \frac{\kappa}{\sqrt{3} v_h L_1 L_2} \sum_p [\phi_-(-p)\phi_-(p) + \phi_+(-p)\phi_+(p) - \phi_-(-p)\phi_+(p)H(-p) - \phi_+(-p)\phi_-(p)H(p)], \quad (\text{A6})$$

where

$$H(p) = e^{-ip_1} \frac{1}{3} \left(1 + 2e^{i\frac{3p_1}{2}} \cos \frac{\sqrt{3}p_2}{2} \right). \quad (\text{A7})$$

From (A6) we derive the propagators:

$$\begin{aligned} \langle \phi_-(k)\phi_-(q) \rangle &= \langle \phi_+(k)\phi_+(q) \rangle = v_h \frac{\sqrt{3}}{\kappa} \frac{1}{\Delta(k)} \delta_{k+q,0}, \\ \langle \phi_+(k)\phi_-(q) \rangle &= v_h \frac{\sqrt{3} H(k)}{\kappa \Delta(k)} \delta_{k+q,0}, \end{aligned} \quad (\text{A8})$$

where

$$\Delta(k) = \frac{8}{9} \left[2 - \cos \frac{\sqrt{3}}{2} k_2 \left(\cos \frac{3}{2} k_1 + \cos \frac{\sqrt{3}}{2} k_2 \right) \right]. \quad (\text{A9})$$

When x_+ and x_- are the ends of the same link, i.e. $|x_+ - x_-| = 1$, one can easily prove that

$$\langle \phi_+(x_+)\phi_-(x_-) \rangle - \langle \phi_-(x_-)\phi_-(x_-) \rangle = -\frac{1}{3\kappa}. \quad (\text{A10})$$

The nearest-neighbour action of chiral models on the honeycomb lattice is

$$S_h = -\frac{\sqrt{3}}{T} \sum_{\text{links}} 2\text{Re Tr} [U_l U_r^\dagger], \quad U \in SU(N), \quad (\text{A11})$$

where l, r indicate the sites at the ends of each link. The perturbative expansion is performed by setting

$$U = e^{iA} , \quad A = \sum_a T_a A_a , \quad (\text{A12})$$

(T_a are the generators of the $SU(N)$ group and A_a are $N^2 - 1$ real fields) and expanding U in powers of A . The action S_h becomes

$$S_h = \frac{\sqrt{3}}{T} \sum_{\text{links}} \left[\text{Tr}(A_l - A_r)^2 + \frac{1}{4} \text{Tr}(A_l^2 - A_r^2)^2 - \frac{1}{3} \text{Tr}(A_l - A_r)(A_l^3 - A_r^3) + O(A^6) \right] . \quad (\text{A13})$$

The change of variables (A12) requires the introduction of an additional term in the action

$$S_m = \frac{N}{12} \sum_{\text{sites}} \text{Tr} A_i^2 + O(A^4) . \quad (\text{A14})$$

Then following the recipe illustrated in the Gaussian example, we rewrite the field $A^a(x_s)$ in terms of two new fields $A_-^a(x_-)$ and $A_+^a(x_+)$, whose propagators can easily be derived from those of the Gaussian models, cfr. (A8). We are now ready to perform weak coupling calculations.

Given the free energy per site

$$F(\beta) = \frac{1}{n_s N^2} \ln \int \prod_x dU(x) \exp(-S_h) , \quad (\text{A15})$$

where n_s is the number of sites, the internal energy (per link) can be obtained by

$$E = 1 - \frac{1}{3} \frac{dF(\beta)}{d\beta} . \quad (\text{A16})$$

The internal energy up to two loops is given by Eq. (20).

In order to evaluate the ratio between the Λ -parameters of the \overline{MS} renormalization scheme and the honeycomb lattice regularization, we calculated the correlation function

$$G(T, x_+ - y_+) = \frac{1}{N} \langle \text{Re Tr} [U(x_+) U(y_+)^\dagger] \rangle . \quad (\text{A17})$$

In the x -space we obtained (neglecting $O(a)$ terms)

$$G(T, x, a) = 1 + \frac{N^2 - 1}{2N} T F(a/x) + O(T^2) , \quad (\text{A18})$$

where

$$F(a/x) = \frac{1}{2\pi} \left(\ln \frac{a}{x} - \gamma_E - \ln 2 \right) . \quad (\text{A19})$$

In the p space

$$\tilde{G}(T, p, a) = \frac{N^2 - 1}{2N} \frac{T}{p^2} \left[1 + \frac{N^2 - 2}{4N} T \left(D(ap) + \frac{1}{3\sqrt{3}} \right) + O(T^2) \right] , \quad (\text{A20})$$

where

$$D(ap) = \frac{1}{2\pi} (\ln ap - 2 \ln 2) . \quad (\text{A21})$$

The above results required, beside the relation (A10), the calculation of the following integrals:

$$\int_{-\frac{2\pi}{3}}^{\frac{2\pi}{3}} \frac{dk_1}{2\pi} \int_{-\frac{\pi}{\sqrt{3}}}^{\frac{\pi}{\sqrt{3}}} \frac{dk_2}{2\pi} \frac{e^{ikx} - 1}{\Delta(k)} = F(a/x) + O\left(\frac{a}{x}\right) , \quad (\text{A22})$$

$$\int_{-\frac{2\pi}{3}}^{\frac{2\pi}{3}} \frac{dk_1}{2\pi} \int_{-\frac{\pi}{\sqrt{3}}}^{\frac{\pi}{\sqrt{3}}} \frac{dk_2}{2\pi} \frac{\Delta(p) - \Delta(k) - \Delta(k+p)}{\Delta(k)\Delta(k+p)} = 2D(ap) + O(ap) , \quad (\text{A23})$$

where the extremes of integration are chosen to cover the appropriate Brillouin zone, which can be determined from the finite lattice momenta (A3).

The next step consists in determining the renormalized functions $Z_t^{\overline{MS}}(T, a\mu)$ and $Z_U^{\overline{MS}}(T, a\mu)$ that satisfy the equations

$$\begin{aligned} G_R^{\overline{MS}}(t, x, \mu) &= Z_U^{\overline{MS}}(T, a\mu)^{-1} G(T, x, a) , \\ T &= Z_t^{\overline{MS}}(T, a\mu) t , \end{aligned} \quad (\text{A24})$$

where t and $G_R^{\overline{MS}}(t, x, \mu)$ are respectively the coupling and the correlation function renormalized in the \overline{MS} scheme. In the \overline{MS} renormalization scheme we have [2]

$$\begin{aligned} G_R^{\overline{MS}}(t, x\mu = 2e^{-\gamma E}) &= 1 + O(t^3) , \\ \tilde{G}_R^{\overline{MS}}(t, \frac{p}{\mu} = 1) &= \frac{N^2 - 1}{2N} \frac{t}{p^2} [1 + O(t^2)] . \end{aligned} \quad (\text{A25})$$

Then by imposing Eqs. (A24) we obtain

$$Z_t^{\overline{MS}}(T, a\mu) = 1 + T \frac{N}{8\pi} (\ln a\mu + d) + O(T^2) , \quad (\text{A26})$$

where

$$d = -2 \ln 2 - \frac{N^2 - 2}{N^2} \frac{2\pi}{3\sqrt{3}} . \quad (\text{A27})$$

The constant d determines the ratio $\Lambda_{\overline{MS}}/\Lambda_h$, indeed

$$\frac{\Lambda_{\overline{MS}}}{\Lambda_h} = e^{-d} = 4 \exp\left(\frac{N^2 - 2}{N^2} \frac{2\pi}{3\sqrt{3}}\right) . \quad (\text{A28})$$

For the interested reader we mention that Eqs. (A22-A23) may be derived from the following exact result

$$\begin{aligned} &\int_{-\frac{2\pi}{3}}^{\frac{2\pi}{3}} \frac{dk_1}{2\pi} \int_{-\frac{\pi}{\sqrt{3}}}^{\frac{\pi}{\sqrt{3}}} \frac{dk_2}{2\pi} \frac{1}{\Delta(k) + m^2 \left(1 + \frac{m^2}{8}\right)} = \\ &\frac{1}{2\pi} \left(1 + \frac{3}{8}m^2\right)^{-3/2} \left(1 + \frac{1}{8}m^2\right)^{-1/2} K \left[\left(1 + \frac{1}{4}m^2\right)^{1/2} \left(1 + \frac{3}{8}m^2\right)^{-3/2} \left(1 + \frac{1}{8}m^2\right)^{-1/2} \right] . \end{aligned} \quad (\text{A29})$$

REFERENCES

- [1] P. Rossi and E. Vicari, Phys. Rev. **D 49** (1994) 1621.
- [2] P. Rossi and E. Vicari, Phys. Rev. **D 49** (1994) 6072; **D 50** (1994) 4718 (E).
- [3] M. Campostrini, P. Rossi and E. Vicari, “Asymptotic Scaling from Strong Coupling”, Pisa preprint IFUP-TH 36/94.
- [4] M. Campostrini, P. Rossi and E. Vicari, “Strong coupling expansion of chiral models”, Pisa preprint IFUP-TH 63/94.
- [5] M. Campostrini, P. Rossi and E. Vicari, “Large-N phase transition in lattice 2-d principal chiral models”, Pisa preprint IFUP-TH 56/94.
- [6] F. Green and S. Samuel, Phys. Lett. **103B**, 110 (1981).
- [7] G. Parisi, in High Energy Physics 1980, Proceedings of the XXth Conference on High Energy Physics, Madison Wisconsin, 1980, edited by L. Durand and L. G. Pondrom, AIP Conf. Proc. No.68 (AIP, New York, 1981).
- [8] J. Balog, S. Naik, F. Niedermayer, and P. Weisz, Phys. Rev. Lett. **69**, 873 (1992).
- [9] D. L. Hunter and G. A. Baker Jr., Phys. Rev. **B 49** (1979) 3808.
- [10] M. E. Fisher and H. Au-Yang, J. Phys. **A12** (1979) 1677.
- [11] A. J. Guttmann, J. Phys. **A20** (1987) 1839.

FIGURES

FIG. 1. Specific heat vs. β . The dashed and solid lines represent the plain strong coupling series and its resummation. The estimate of the critical β is indicated by vertical dotted lines. When error bars are not visible, they are smaller than the symbol size.

FIG. 2. Magnetic susceptibility vs. β . The dashed and solid lines represent the plain strong coupling series and its resummation respectively. The estimate of the critical β is indicated by the vertical dotted lines.

FIG. 3. μ_s/μ_d vs. $\xi_G \equiv 1/M_G$.

FIG. 4. μ_s/M_G vs. $\xi_G \equiv 1/M_G$. The dashed lines represents the continuum limit result from Monte Carlo data.

FIG. 5. Asymptotic scaling test by using strong-coupling estimates. The dotted line represents the exact result (15).

FIG. 6. μ_1/μ_2 vs. $\xi_G \equiv 1/M_G$ for the honeycomb lattice.

FIG. 7. μ_1/M_G vs. $\xi_G \equiv 1/M_G$ for the honeycomb lattice. The dashed lines represents the continuum limit result from Monte Carlo data.

FIG. 8. Asymptotic scaling test for the honeycomb lattice by using strong-coupling estimates. The dotted line represents the exact result (24). The full line corresponding to the ratio $M_G/\Lambda_{h,E}$ was constructed by resumming the involved strong coupling series.

TABLES

TABLE I. Resummation of the strong coupling series of the specific heat. We analyze the series of $\beta^{-2}C$ expressed in terms of β^2 , cf. Eq. (8), for which $M = 8$. We report the first singularity in the real axis, $\beta_0 \equiv \sqrt{x_0}$, and the corresponding exponent versus L, K , and J .

L	K	J	β_0	γ
2	2	2	0.30598	0.252
2	3	1	0.30566	0.227
2	1	3	0.30586	0.245
2	0	4	0.30563	0.228
2	4	0	0.30569	0.228
3	2	1	0.30697	0.280
3	1	2	0.30591	0.250
3	3	0	0.30568	0.228
3	0	3	0.30619	0.277
4	1	1	0.30508	0.183
4	2	0	0.30475	0.166
4	0	2	0.30570	0.233
5	1	0	0.30562	0.222
5	0	1	0.30588	0.241
6	0	0	0.30564	0.225

TABLE II. Analysis of the series of $d \ln \chi / d\beta$ and $d \ln \beta M_G^2 / d\beta$. For some set of L, K and J we report the range of values of γ corresponding to the range of zero values 0.3055 – 0.3061.

	L	K	J	γ
$\frac{d \ln \chi}{d\beta}$	4	5	4	0.20-0.24
	4	4	5	0.28-0.31
	5	4	4	0.23-0.27
	5	5	3	0.22-0.26
	6	3	4	0.22-0.26
	6	4	3	0.23-0.27
$\frac{d \ln(\beta M_G^2)}{d\beta}$	4	4	4	0.23-0.26
	5	4	3	0.26-0.30
	5	3	4	0.07-0.12
	6	3	3	0.10-0.15

TABLE III. Resummation of the 24th order strong coupling series of the specific heat for the honeycomb lattice. We analyze the series of $\beta^{-2}C$ expressed in terms of β^2 , cf. Eq. (18), for which $M = 12$. We report the first singularity in the real axis, $\beta_0 \equiv \sqrt{x_0}$, and the corresponding exponent versus L, K , and J .

L	K	J	β_0	γ
3	4	3	0.43386	0.162
3	3	4	0.43389	0.165
4	3	3	0.43393	0.167
4	4	2	0.43398	0.171
4	2	4	0.43381	0.161
5	3	2	0.43387	0.163
5	2	3	0.43415	0.185
5	4	1	0.43397	0.171
5	1	4	0.43495	0.240
6	2	2	0.43312	0.101

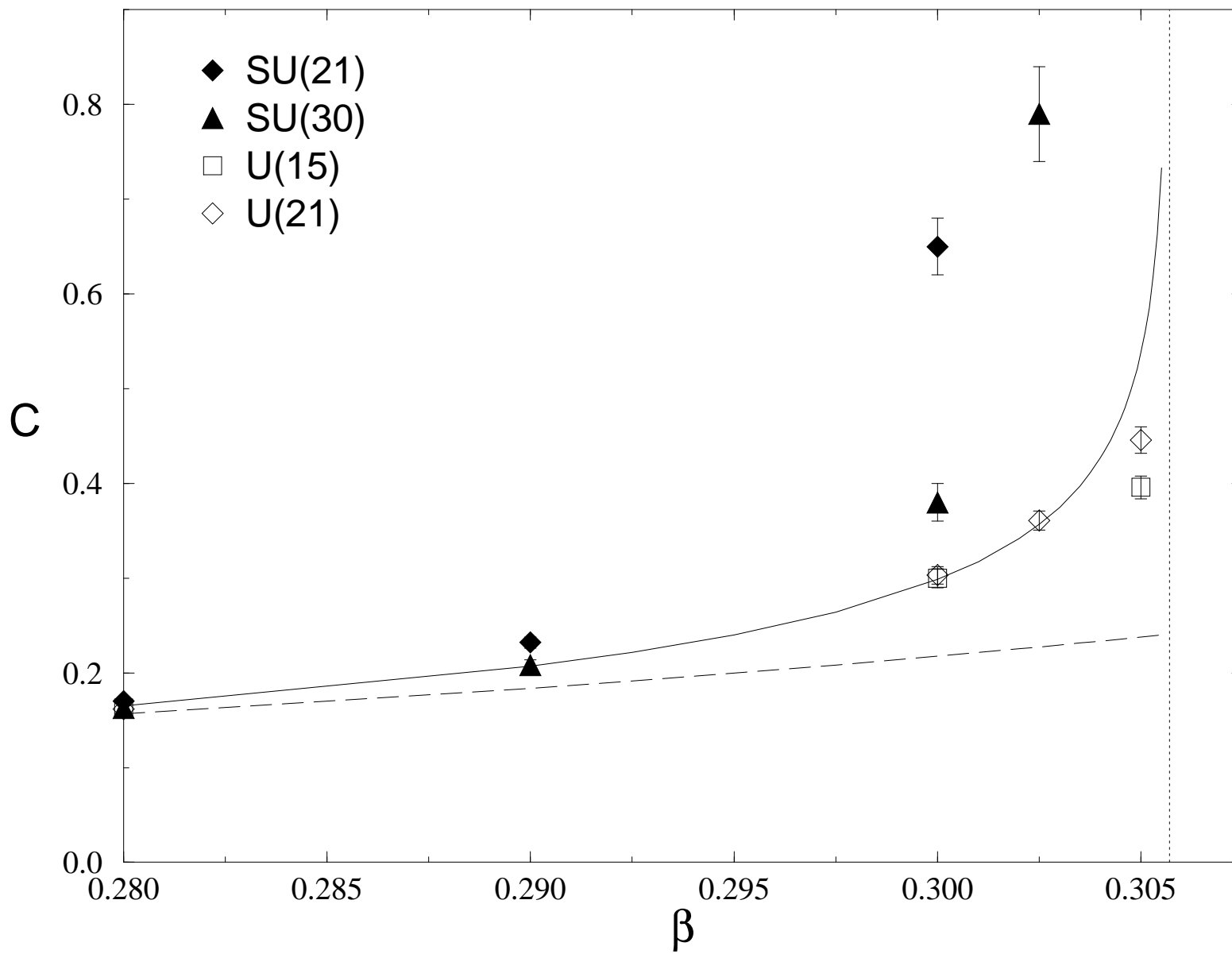
TABLE IV. Analysis of the series of $d \ln \chi / d\beta$ (19th order) and $d \ln \beta M_G^2 / d\beta$ (18th order) for the honeycomb lattice. For some set of L, K and J we report the range of values of γ corresponding to the range of zero values 0.4338 – 0.4340.

	L	K	J	γ	
$\frac{d \ln \chi}{d\beta}$	6	6	6	0.15-0.16	
	6	7	5	0.14-0.15	
	6	5	7	0.14-0.15	
	7	5	6	0.15-0.16	
	7	6	5	0.30-0.30	
	8	5	5	0.15-0.16	
	$\frac{d \ln(\beta M_G^2)}{d\beta}$	6	6	5	0.21-0.22
		6	5	6	0.22-0.23
7		5	5	0.21-0.22	
8		4	5	0.17-0.18	
8		5	4	0.22-0.24	

This figure "fig1-1.png" is available in "png" format from:

<http://arxiv.org/ps/hep-lat/9412101v1>

Figure 1



This figure "fig2-1.png" is available in "png" format from:

<http://arxiv.org/ps/hep-lat/9412101v1>

This figure "fig3-1.png" is available in "png" format from:

<http://arxiv.org/ps/hep-lat/9412101v1>

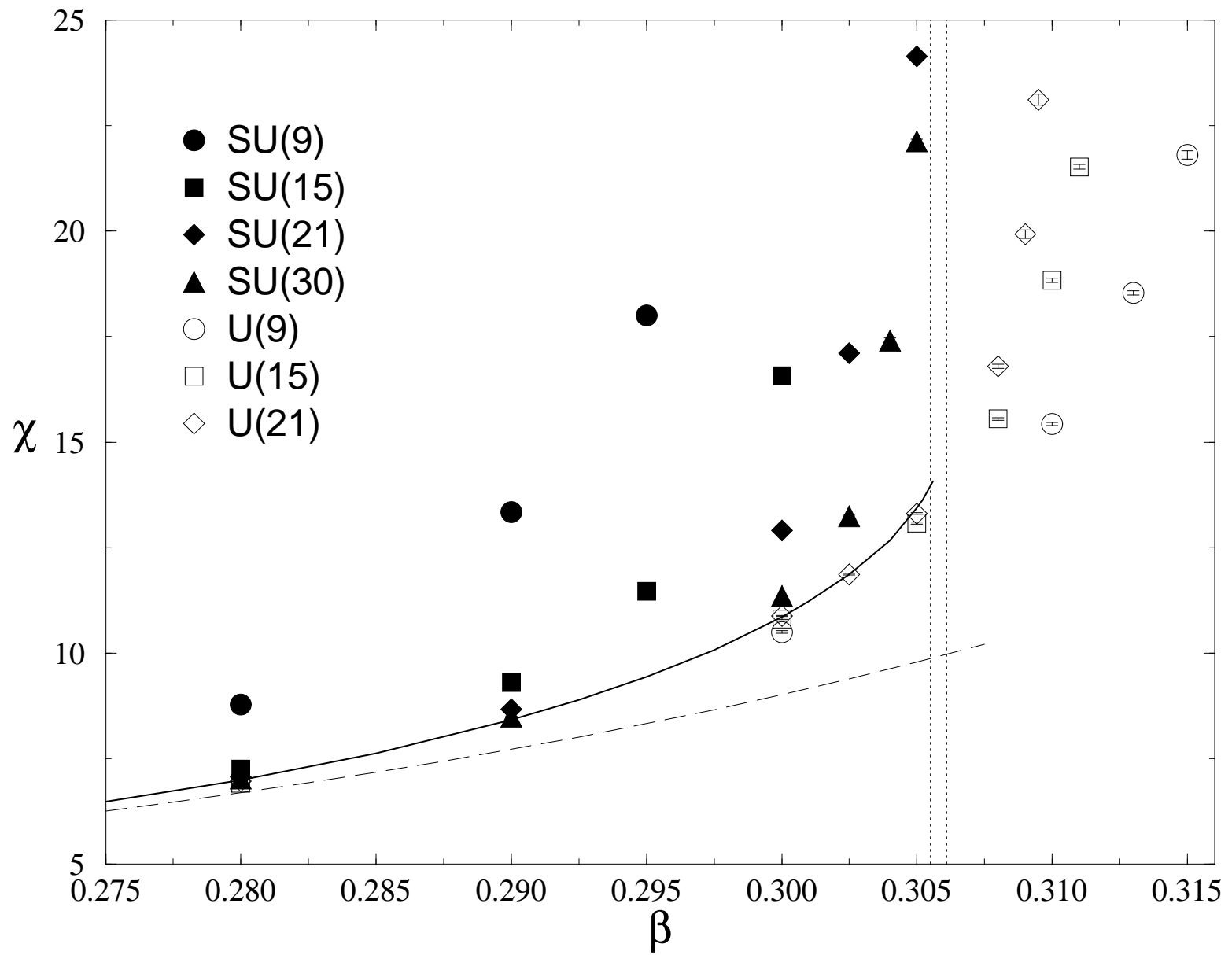
This figure "fig1-2.png" is available in "png" format from:

<http://arxiv.org/ps/hep-lat/9412101v1>

This figure "fig2-2.png" is available in "png" format from:

<http://arxiv.org/ps/hep-lat/9412101v1>

Figure 2



This figure "fig3-2.png" is available in "png" format from:

<http://arxiv.org/ps/hep-lat/9412101v1>

This figure "fig1-3.png" is available in "png" format from:

<http://arxiv.org/ps/hep-lat/9412101v1>

This figure "fig2-3.png" is available in "png" format from:

<http://arxiv.org/ps/hep-lat/9412101v1>

Figure 3

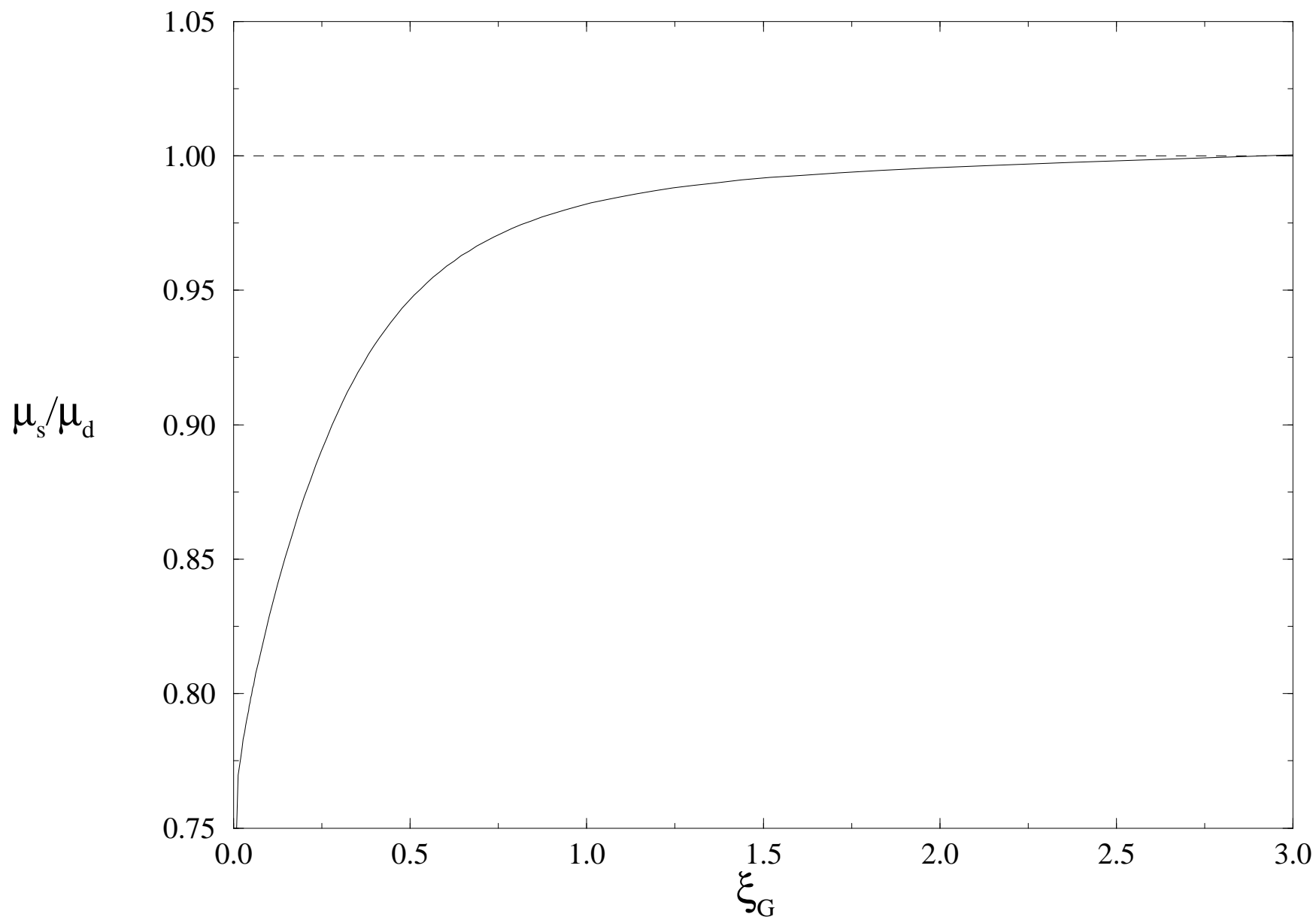


Figure 4

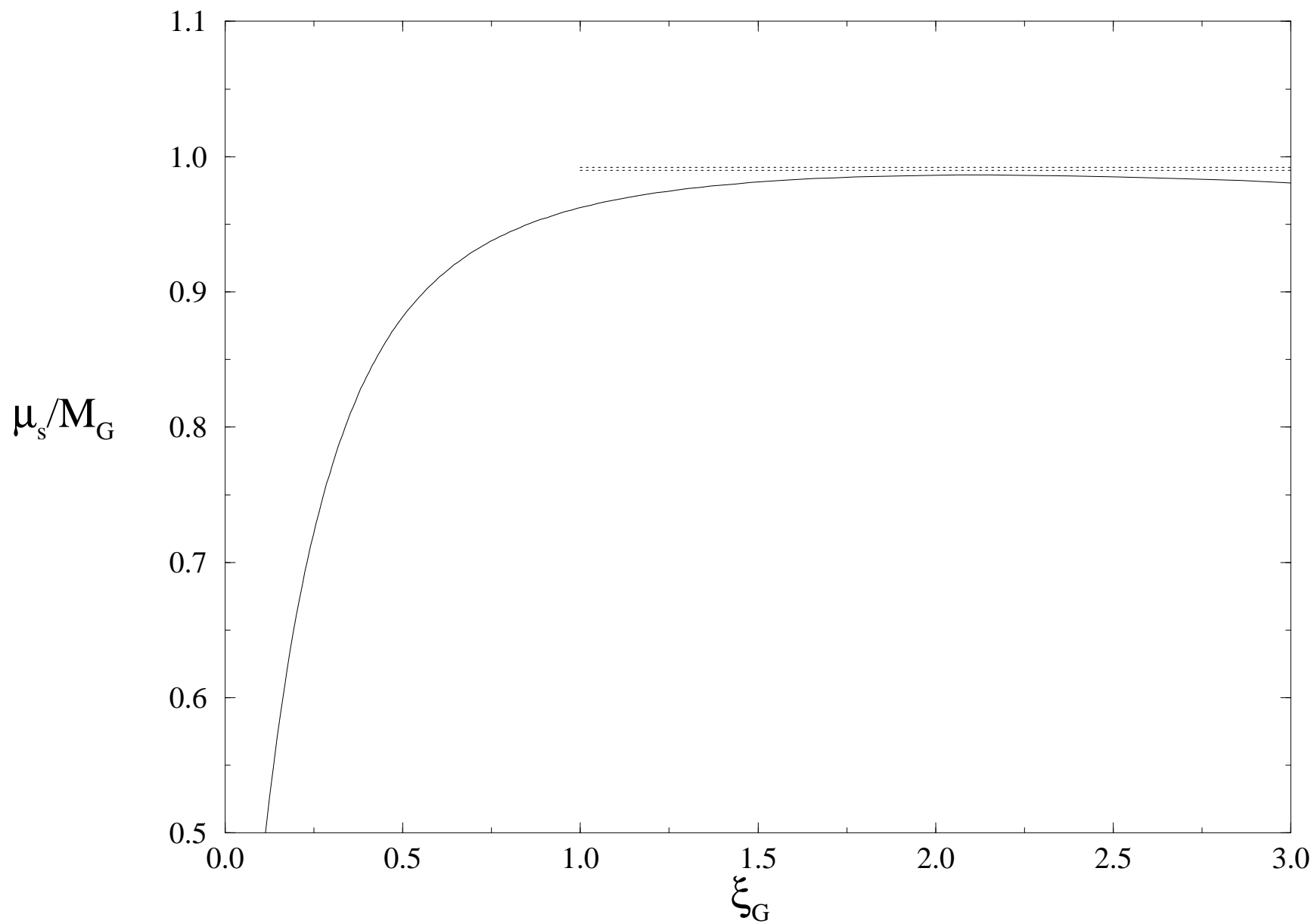


Figure 5

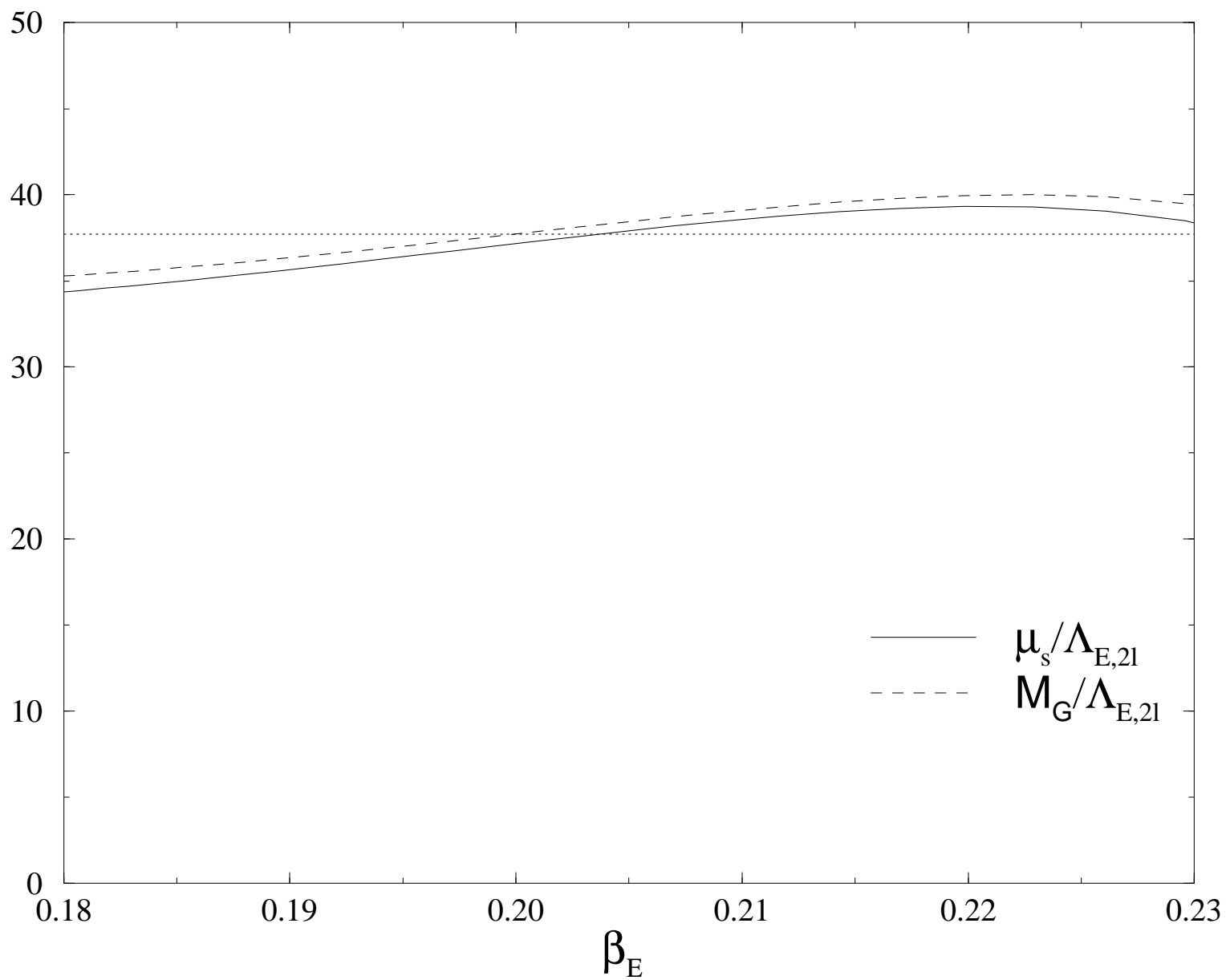


Figure 6

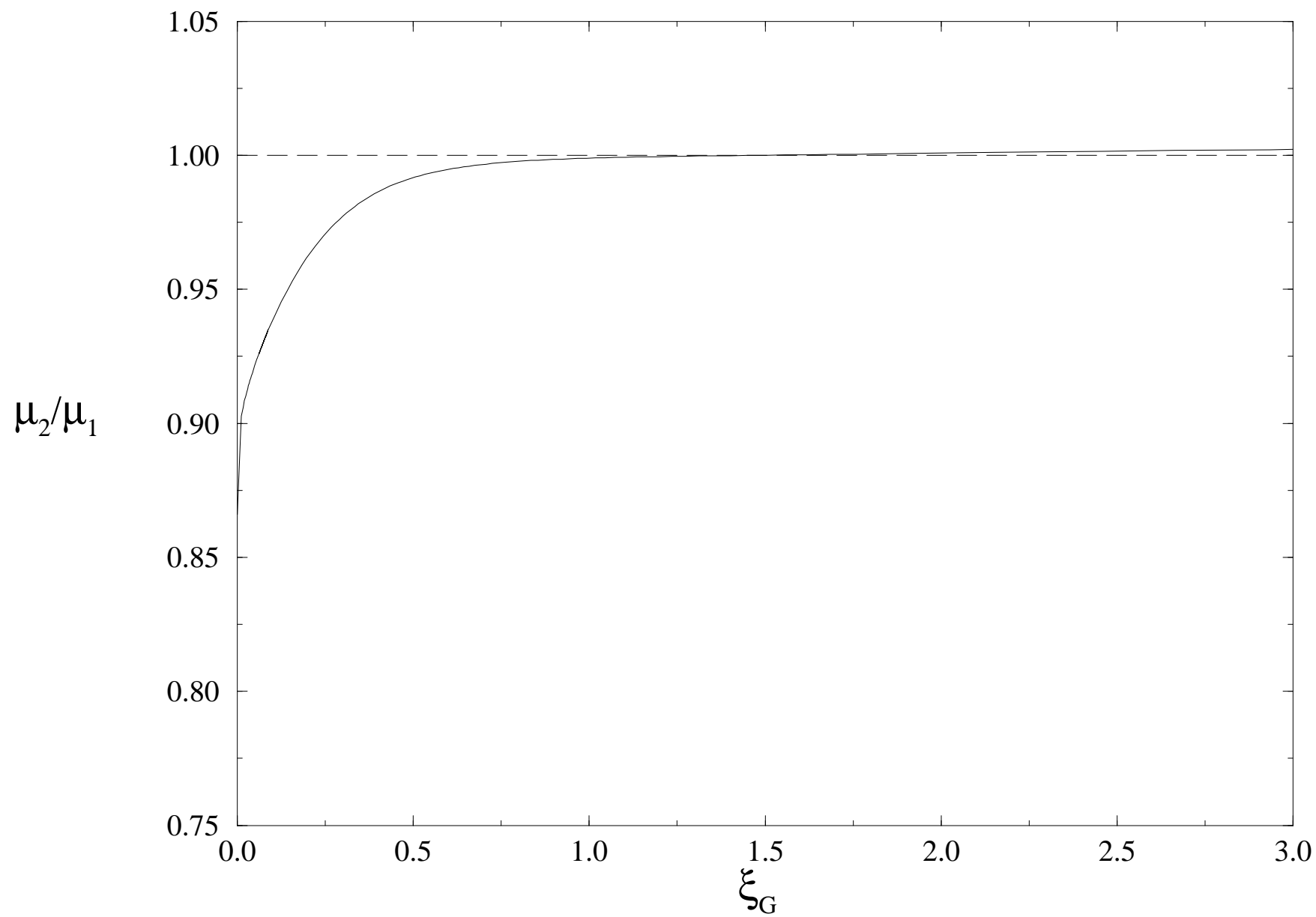


Figure 7

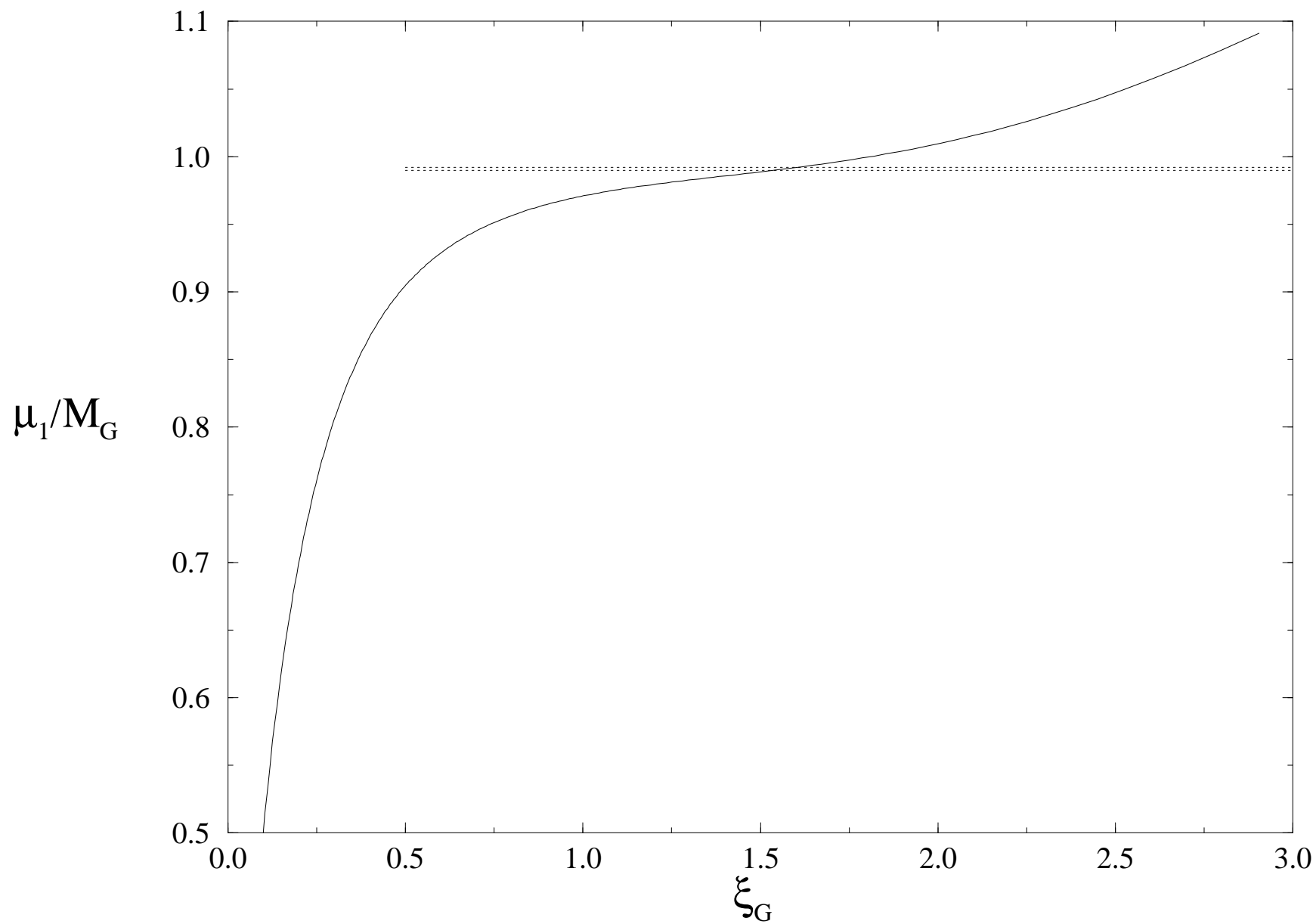


Figure 8

